Available online at www.sciencedirect.com
SCIENCE DIRECT®
International Journal of Thermal Sciences 41 (2002) 1077–1087
International Journal of Thermal Sciences
www.elsevier.com/locate/ijts

Steam flow through the volumetrically heated particle bed

I.V. Kazachkov [a,*], M.J. Konovalikhin [b]

[a] *Division of Heat and Power Technology, Royal Institute of Technology, Brinellvägen 60, SE-100 44 Stockholm, Sweden*
[b] *Division of Nuclear Power Safety, Royal Institute of Technology, Drottning Kristinas Väg 33A, SE-100 44 Stockholm, Sweden*

Received 16 June 2001; accepted 19 November 2001

Abstract

The paper is devoted to the problem of ex-vessel debris bed coolability, in particular, coolability and quenching of a particulate corium debris bed by water. A number of experiments were performed in the POMECO (POrous MEdia COolability) facility to measure the dry out heat flux in a self-heated bed. A mathematical model for the description of flow of a compressible fluid (steam) through the volumetrically heated porous bed with particular consideration of the non-thermal local equilibrium is formulated and solved numerically using the split step method. It is shown that initial thermodynamic perturbations which, if they grow, will lead to a temperature escalation at a specific location. Furthermore, the data from the RIT (Royal Institute of Technology) POMECO (POrous MEdia COolability) experiments are used for the validation of the model.

Keywords: Severe accident; Particle bed; Coolability; Dryout; Downcomer

1. Introduction and background

Coolability of a heat-generating porous beds has been of concern, since the LMFBR (Liquid Metal Fast Breeder Reactor) days. In the LWR (Light Water Reactor) severe accident scenario, particulate debris beds are formed when corium melt comes in contact with water. This may occur in-vessel in the lower head when melt is discharged from the core to the lower head (e.g., TMI-2 (Three-Miles-Island reactor)), and, may occur ex-vessel, when melt is discharged from the vessel failure site to the containment. Some containment cavities are designed to remain dry (German PWR), however most others will have varying depths of water. The Swedish BWRs (Boiling Water Reactor), in particular, employ the severe accident management (SAM) scheme in which a deep water pool is established in the lower dry-well to fragment the melt into, hopefully, a coolable debris bed. The melt-water interaction scenario will, most probably, produce a stratified bed, quite akin to that found in the FARO tests [1]. The small size particles will be lifted, by the steam produced, into the containment atmosphere and will later on deposit as a dense layer on top. The dryout heat flux as the limiting parameter for steady state removal of the decay heat by boiling of the coolant has been the subject of many theoretical and experimental investigations during the last two decades. The long-term coolability of debris beds is essential to keep the bed temperatures below the melting temperatures of the bed.

An early theoretical and experimental study of the thermalhydraulic characteristics of single phase flow through a volumetrically heated porous layer is that of Choudhary and El-Wakil [2]. They solved the coupled linear energy equation for the solid and gas phase using an implicit modified Crank–Nicholson method.

Dhir and Catton [3] made experimental observations of the dryout heat fluxes for inductively heated particulate beds cooled from the top. This study dealt with two bed configurations, shallow and deep. Different mechanisms for the dryout in these beds were identified. It was concluded that the deep bed dries out at a particular section primarily in the lower regions of the bed where gravity can no longer maintain the flow rate necessary to compensate for the evaporation rate, or, in other words, when the evaporation rate is greater than what can be sustained by the average downward superficial velocity of the coolant. Some semi-theoretical correlations based on the proposed hydrodynamic models were developed and validated.

* Corresponding author.
E-mail addresses: ivan@egi.kth.se (I.V. Kazachkov), maxim@ne.kth.se (M.J. Konovalikhin).

1290-0729/02/$ – see front matter
PII: S1290-0729(02)01394-7

Nomenclature

p	pressure	Pa
K	permeability coeffcient	m^2
C	specific heat capacity	$J{\cdot}kg^{-1}{\cdot}K^{-1}$
T	temperature	K
k	thermal conductivity	$W{\cdot}m^{-1}{\cdot}K^{-1}$
a	thermal diffusivity	$m^2{\cdot}s^{-1}$
Q_Σ	specific solid-liquid interface heat flux	$W{\cdot}m^{-3}$
Q_V	heat source	$W{\cdot}m^{-3}$
R	universal gas constant	$m^3{\cdot}Pa{\cdot}mol^{-1}{\cdot}K^{-1}$
t	time	sec
H	height of the system	m
u	horizontal velocity component	$m{\cdot}s^{-1}$
w	vertical velocity component	$m{\cdot}s^{-1}$
x	horizontal coordinate	m
z	vertical coordinate	m
g	gravitational acceleration	$m{\cdot}s^{-2}$
Pe	Peclet number	
Re	Reynolds number	
Da	Darcy number	
Gr	Grasshoff number	
Nu	Nusselt number	
Fo	Fourier number	
Ra	Rayleigh number	

Greek symbols

ρ	density	$kg{\cdot}m^{-3}$
σ	stress tensor	$N{\cdot}m^{-1}$
μ	dynamic viscosity	Pa·s
α	porosity	
β	thermal expansion	K^{-1}

Subscripts/Superscripts

0	values at specified constant temperature
1	fluid phase
2	solid phase
3	ambient media
k	layer number

Vasiliev and Mairov [4,5] analyzed heat transfer, pressure drop and stability characteristics of a volumetrically heated porous layer cooled with forced flow evaporation. Depending on the physical properties of the coolant, they divided the porous layer into three regions—subcooled, saturated two phase mixture and superheated steam. For each region, they solved the energy equations with appropriate boundary and interfacial conditions to obtain temperature distribution in the solid and the fluid. But the of flow direction in this study is normal to the body force, whereas in physical situations of interest in reactor safety, the gravity acts in a direction parallel to the flow.

Later, Naik and Dhir [6] experimentally investigated a volumetrically heated porous layer with coolant flowing through that. The purpose of this work was to obtain the data for the steady state temperature profile and pressure drop of an evaporating two-phase coolant flowing vertically. A model for the temperature profile, based on the solution of the one-dimensional energy equations for the particles and the coolant with assumption of no differences between the solid and liquid temperatures, was developed. The two-phase pressure drop was evaluated by a separated flow model based on the empirical relations obtained from the experiments. In this model, the void fraction was correlated as a function of the flow quality and mass flow rate. The model worked reasonably well for water-steam at atmospheric pressure, however not as well for fluid mixtures with a higher vapor/liquid volume ratio.

Hofmann [7] presented the results of experimental and analytical investigation on dryout heat flux in inductively heated beds for, both, top and top-and-bottom fed conditions. His model, which calculates the heat flux as a function of the saturation by solving the conservation equations for momentum, mass and energy, gives a saturation distribution for dryout condition. But no satisfactory comparison was achieved with experimental data.

Considerable interest was generated in employing hydrodynamic models for predicting dryout, since, clearly, counter-current flooding generally controls dryout in porous media made up of large size particles. Several experimental and analytical studies on hydrodynamic aspects of two-phase flow through porous media were performed, as summarized by Schulenberg and Müller [8]. It is unfortunate that most of these studies were carried out for the idealized condition of a one-dimensional homogeneous porous layer, whereas those encountered in actual practice are multi-dimensional and may be composed of regions with widely varying permeabilities and heating conditions.

Tsai in [9] measured dryout heat fluxes in axi-symmetric porous layers with partial volumetric heating. His numerical solution was obtained by a finite difference scheme without the interfacial drag term. Capillary pressure was included in his solutions through the use of the Lawrett function. In this work the solutions were obtained with “pseudo stream functions” to include the source terms due to the volumetric heating. But such an approach exists only for certain distribution of volumetric heating in the porous layers.

A hydrodynamic model was developed by Tung and Dhir [10] to predict void fractions and pressure gradient for one-dimensional two-phase flow through porous media. The particle-gas drag, particle-liquid drag and liquid-gas interfacial drag were evaluated theoretically for the flow configurations associated with different flow regimes. The drag models were then employed in conjunction with force balances on the two phases to obtain the void fraction and pressure gradient as functions of liquid and gas superficial

velocities. This mechanistic model was modified and solved numerically in [11] by the same authors. The numerical scheme, based on the finite element model, called for elimination of velocities in favor of pressure and void fraction to predict dryout heat flux. The finite element model allowed the existence of several regions of different permeabilities in the domain. Solutions were obtained both in two-dimensional cartesian and in the axi-symmetric coordinate system.

The modeling approach of channeling of self-heated particle beds is exemplified by the Lipinski model [12]. It was assumed in this model that the vapor pressure at the bottom of a channel is sufficient to offset the weight of the overlying particles plus liquid and the flow resistances in the channeled region are neglegible. Later on, Lipinski [13] introduced the idea of a sticking factor S_f, which means that the vapor pressure must be S_f times the overlying bed pressure at the bottom of a channel. However, it appears that a nondimensionalization of this sticking pressure leads straightforwardly to the sticking factor concept. The sticking factor model relies upon the analysis of the motion of particles caused by the upward displacement of a piston through the bed. Such a simulation is regarded as representative of the onset of channeling. Stubos and Buchlin [14] extended Lipinski's model by applying a force balance to a single bottom particle which included the weight of the overlying particles and the friction force. In details, they investigated [15] the behavior of vapor channels traversing the upper part of a boiling, unconstricted, homogeneous debris bed and suggested a theoretical model for the dryout heat flux in a channeled bed. A multi-dimensional mathematical model for numerical analysis was developed and presented in [16] by Stubos and Buchlin assuming local thermal equilibrium (LTE) between the solid and liquid phases (thermally homogeneous medium). But this assumption may not be satisfactory for the step change problems in which, during the early stages of the transport processes there may be considerable differences between the temperatures of the flowing fluid and solid particles. This is also true even during the later stages of the transport processes in high speed flows in which the fluid to solid interaction time may not be large enough to bring the temperatures of the fluid and solid phases close enough for LTE to be a reasonable assumption.

Non-thermal equilibrium flow through a porous bed is a subject of essential interest. Sözen and Vafai [17] presented a general set of volume-averaged governing equations for non-thermal equilibrium condensing forced flow through a latent heat storage porous media and comprehensive numerical investigations of the phenomenon were carried out. Kuznetsov [18] made such an analysis based on solution, by the perturbation technique, of the full energy equations for incompressible fluid and solid phases, without neglecting any terms in the equations. He showed that the temperature between the fluid and solid phases in a semi-infinite packed bed forms a wave localized in space. Later on, he investigated [19,20] the thermal behavior of the three-dimensional porous bed during non-thermal equilibrium fluid flow through it, with assumption of constant thermal, physical and transport properties.

The present work describes the determination of the dryout location by introducing initial thermodynamic perturbations which, if they grow, will lead to a temperature escalation at a specific location. An analysis of the steam thermal behavior in the two-dimensional homogeneous and stratified porous beds with temperature dependent thermal conductivity coefficient has been performed.

2. Experimental study

An experimental investigation named POMECO (POrous MEdiia COolability) on dryout heat flux of a particulate bed was performed. Both homogeneous and stratified debris beds were recently employed at RIT and some results were reported [21].

The objectives of the POMECO program are to provide the data base and the models to resolve the following issues:

- Is a deep, stratified, low-porosity, bed coolable at low pressure in a deep pool of water?
- Can the dryout heat flux be enhanced, i.e., coolability potential enhanced?
- What are the feasible back-fits and what is the enhancement in the dryout heat flux?

Focus is placed on low porosity, small particle size and relatively large scale debris beds. Bed stratification is an important parameter for investigations. Most debris bed coolability experiments have been performed with steel balls of different size, generally heated by induction. We have taken a different approach. Since corium debris have a particle size distribution and are more like sand, our debris beds were built with sand of different particle size distributions, heated with a network of thin heaters, distributed uniformly in the sand bed to produce uniform volumetric heat generation. The experiments were conducted on low porosity beds, since they are the most difficult to cool with top flooding. For enhancement of the dryout heat flux, we reasoned that since water addition from bottom has been shown to be a more efficient mode of cooling in earlier experiments, as well as in the COMET experiments [22] for melt coolability, water should be channeled to the bottom of the debris bed. A similar approach was proposed by late Prof. Becker of RIT [23], who performed some small scale scoping experiments. The downcomer(s) were built in the debris bed which would channel the water from the water overlayer to the bottom of the bed and develop a two phase natural circulation flow loop, providing greater mass flow rate in the bed. The following parameters were varied in the experients: (i) the downcomer flow area, (ii) downcomer geometry, e.g., with holes along bed height.

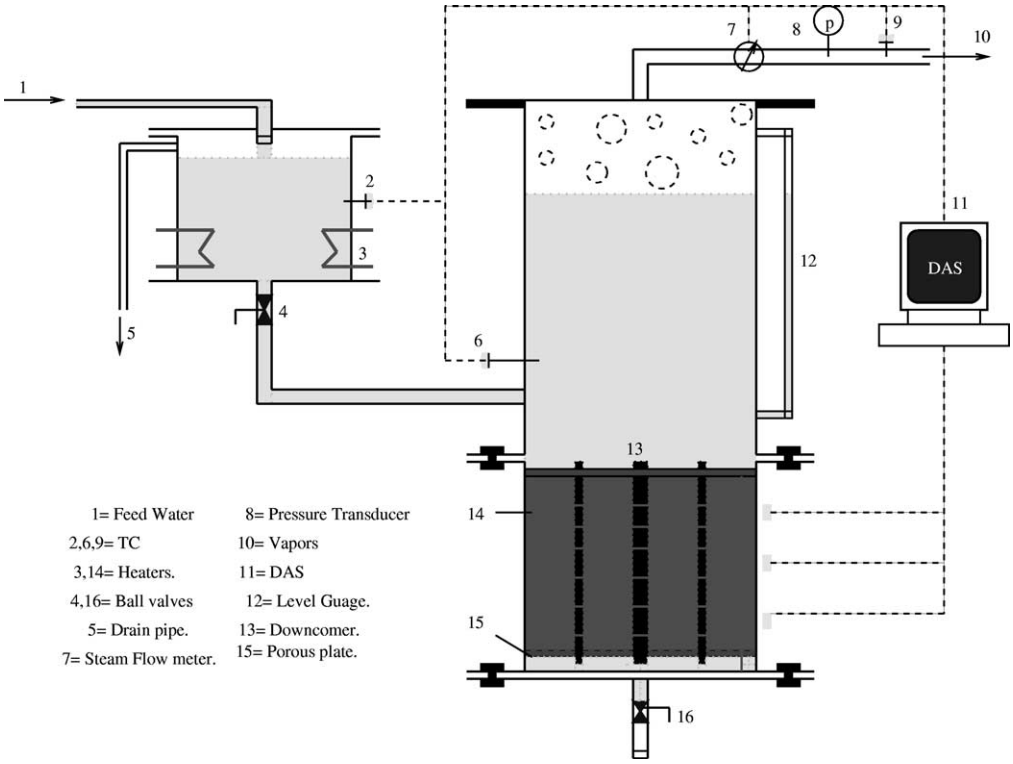

Fig. 1. Schematic of the POMECO facility.

2.1. Experimental facility

The schematic of POMECO facility is shown in Fig. 1 and described in more detail in [21]. The POMECO facility consists of water supply system, test section, heater system, measurement and DAS systems.

Different size sand particles are chosen to construct the porous particle bed with different characteristics, e.g., mean particle size, porosity, and stratification. The top surface of the particle bed is covered by grids with small size holes to avoid channel formation in the particle bed and fly off of small sand particle.

The test section is a stainless steel vessel whose details are presented in Fig. 1. The cross-sectional area of the test section is 350 × 350 mm rectangular. The height of the lower part is 500 mm and the height of the upper part is 900 mm. The maximum height of the sand can be 450 mm. A porous plate was placed 50 mm above the bottom of the test section to provide enough space for the water coming from the downcomer, for disribution into the sand bed. It is a 350 × 350 stainless steel plate, in which there are about 100 holes with a diameter of 10 mm. The downcomer fixed to the porous plate is a tube of stainless steel with 500 mm height and 30 mm internal diameter, it is fixed on the porous plate. Later, the downcomer was drilled with holes along vertical direction, and then, this number of holes was doubled. Before the sand bed is formed, a grid is placed on this porous plate in order to prevent fine sand particles from falling into the bottom space. A water level gauge is installed in the upper part of the test section to monitor the water level variation during the experiment.

2.2. Experimental results and discussion

Six series of experiments were performed for both homogeneous and stratified particle beds. The effects of porosity, mean particle size, and stratification of the particle bed on the dryout heat flux have been measured. The first test series (homo-1.1, -2.1, -3.1 and strat-1.1, -2.1, -3.1, -4.1) was conducted without downcomer, the second (homo-1.2, -2.2, -3.2 and strat-1.2, -2.2, -3.2, -4.2) with the downcomer, the third (homo-3.3 and strat-1.3, -2.3, -3.3, -4.3) with the downcomer with the holes, the fourth (homo-3.4 and strat-2.4, -4.4) with the downcomer with twice the number of the holes, the fifth (homo-3.5 and strat-2.5, -4.5) with four additional downcomers, which increase the total flow area by a factor of two and the sixth (homo-3.6 and strat-2.6, -4.6) with four downcomers to investigate the influence of the change of downcomer geometry with no change of the flow area.

Three homogeneous sand particle beds are tested, in which the porosities of the particle beds are varied from 0.258 to 0.397, the mean (mass-averaged) particle sizes are smaller than 1 mm.

Table 1 shows the experimental results on the dryout heat flux for the homogeneous particle beds both with and without a downcomer. The predictions of dryout heat flux by Lipinski's zero-dimension model [12] for the particle bed without a downcomer are also listed in this table. It seen that except for the particle beds with very small mean particle sizes

Table 1
Experimental results for homogeneous particle beds

Test number	Sand bed characteristics	Down comer	Dryout h. flux KW·m^{-2}		Enhanc. by dwcm
			Exp.	Lipinsky model	%
homo-1.1	porosity = 0.4, D_{mean} = 0.2 mm	No	90	23	
homo-1.2	same as homo-1.1	Yes	183		104
homo-2.1	porosity = 0.36,	No	222	215	
homo-2.2	same as homo-2.1	Yes	331		49
homo-3.1	porosity = 0.26, D_{mean} = 0.8 mm	No	111	100	
homo-3.2	same as homo-3.1	Yes	202		82
homo-3.3*	same as homo-3.1	Yes	200		80
homo-3.4^{+}	same as homo-3.1	Yes	258		132
homo-3.5	same as homo-3.1	Yes (5)	313		182
homo-3.6	same as homo-3.1	Yes (4)	209		88

(test homo-1.1) the experimental results on dryout heat flux agree quite well with the predictions by Lipinski's model. For the test homo-1.1, the experimental result on dryout heat flux is much higher than the prediction by Lipinski's model, even though the porosity is not low. This indicates that either the Lipinskimodel does not extend to mean particle size of 0.2 mm or for these small particle beds, capillary force contributes substantially to the flow in the bed.

From Table 1 it can also be seen that there is a large enhancement of the dryout heat flux by the downcomer, the natural circulation flow that gets established. Water is channeled to the bottom of the particle bed through the downcomer. The dryout heat flux consists of two parts: one is the contribution from the water penetrations from the top of the particle bed, which is governed by counter-current flooding limitation (CCFL) and is the dryout heat flux of the particle bed without a downcomer; the second is the contribution from the heat transferred to the water channeled to the bottom of the particle bed through the downcomer.

The experimental results show that larger enhancement of dryout heat flux by the downcomer occurs for the particle beds with fine particles or will low porosity. This clearly indicates that the capillary force contributes to the driving head of the natural circulation in the pool. The provision of a downcomer to channel the coolant to the bottom of the bed has a significant effect on the dryout heat flux.

Focus of the stratified bed experiments is on the effects of particle bed characteristics (such as porosity, mean particle size and the thickness of the fine particle layer, resting on the top of another layer) on the dryout heat flux. In all the experiments, the lower particle layer employs the same particle configuration (mean size and porosity).

Table 2 shows the experimental results for the dryout heat flux for the stratified particle beds both with and without a downcomer. Comparing the experiments strat-2.1 and strat-4.1 with experiment homo-3.1, the upper particle layer of experiments strat-2.1 and strat-4.1 is the same as

Table 2
Experimental results for stratified particle beds

Test number	Sand bed characteristics	Down comer	Dryout h. flux KW·m^{-2}	Enhanc. by dwcm
			Experiment	%
strat-1.1	U. layer: H = 130 mm porosity = 0.4, D_{mean} = 0.2 mm L. layer: H = 240 mm porosity = 0.36, D_{mean} = 1 mm	No	87	
strat-1.2	same as strat-1.1	Yes	186	113
strat-1.3	same as strat-1.1	Yes	210	140
strat-2.1	U. layer: H = 130 mm porosity = 0.26, D_{mean} = 0.8 mm L. layer: H = 240 mm porosity = 0.36, D_{mean} = 1 mm	No	54	
strat-2.2	same as strat-2.1	Yes	138	157
strat-2.3	same as strat-2.1	Yes	212	295
strat-2.4	same as strat-2.1	Yes	226	321
strat-2.5	same as strat-2.1	Yes (5)	319	494
strat-2.6	same as strat-2.1	Yes (4)	114	112
strat-3.1	U. layer: H = 240 mm porosity = 0.4, D_{mean} = 0.2 mm L. layer: H = 130 mm porosity = 0.36, D_{mean} = 1 mm	No	55	
strat-3.2	same as strat-3.1	Yes	190	242
strat-3.3	same as strat-3.1	Yes	205	268
strat-4.1	U. layer: H = 240 mm porosity = 0.26, D_{mean} = 0.8 mm L. layer: H = 130 mm porosity = 0.36, D_{mean} = 1 mm	No	122	
strat-4.2	same as strat-4.1	Yes	235	93
strat-4.3	same as strat-4.1	Yes	258	111
strat-4.4	same as strat-4.1	Yes	280	129
strat-4.5	same as strat-4.1	Yes (5)	315	159
strat-4.6	same as strat-4.1	Yes (4)	201	65

the particle bed of experiment homo-3.1, which has low porosity. Experimental results on the dryout heat flux in these three cases (see Tables 1 and 2) show that stratification of the particle beds does not decrease the dryout heat flux. This observation is different from the analytical model and the experimental observation of Lipinski.

The thickness of the fine particle layer has different effect from that of low porosity. Comparing the particle bed configurations of homo-1.1, strat-1.1 and strat-3.1, and experimental results on dryout heat flux for these three experiments in Tables 1 and 2, it appears that the stratification decreases the dryout heat flux a little. The decrease of the dryout heat flux may be caused by the reduction of the porosity at the interface between the layers. However, when the particle size of the upper layer is very small, the capillary force may increase the water penetration

flow. Therefore, the thickness of fine particle layer has little effect on the dryout heat flux.

It can also be seen in Table 2 that the effect of the downcomer on the dryout heat flux is significant. The downcomers can enhance the dryout heat flux from 50 to 600%. Greater enhancement occurs with larger downcomer flow area, as it can be seen from the fifth test series. The sixth test series showed that changing the downcomer geometry with no change of the flow area does not modify the increase in the dryout heat flux.

3. Analysis

3.1. Criteria of consideration of heat removal mechanism

Fig. 2 depicts the schematic diagram of the problem under consideration. A two-dimensional self-heated porous packed bed, wich consists of k homogeneous layers, is filled with the fluid, which moves from the bottom to the top, and is initially at an uniform temperature.

In all POMECO tests temperatures inside the beds were obtained in the range 105–115 °C. Such temperatures require water pressures about 1.3–1.5 bar [24]. But such pressures could not be reached in these tests because of geometry of test section. The overpressure at the bottom is about 0.04 par. Velocities of water penetration in the particle layers calculated with the use of Darcy's law, and which correspond well to experimental data on steam discharge flow rate under dryout conditions (Table 3), show that the whole amount of flowing water will be vaporized at the entrances (layer top and bottom) of penetrating.

The next question is about heat removal mechanism. There is the race: or water takes the heat and the next portion goes to the cooled down area, whether the heat front can propagate faster in this area than the next portion of water will be there. For this purpose the Laplace's solution for linear flow of heat described in [25]. The solution is:

$$v = \frac{1}{2}V\left[\operatorname{erf}\frac{a-x}{2\sqrt{(k^*t)}} + \operatorname{erf}\frac{a+x}{2\sqrt{(k^*t)}}\right]$$

where v and V are variable and constant temperatures respectively, a is character size of the system with constant temperature, $k^* = \frac{k}{\rho \cdot C_p}$ is thermal diffusivity and t is time.

The parameter a was taken 2×10^{-3} m, as a radius of wire of heater, assuming constant temperature in this area. Thermophysical properties are presented below in Table 4:

Calculations for k^* give: $k^*_{\text{sand}} = 2.2 \times 10^{-7}$ m^2·s^{-1}, $k^*_{\text{water}} = 1.6 \times 10^{-7}$ m^2·s^{-1}, $k^*_{\text{steam}} = 2 \times 10^{-5}$ m^2·s^{-1} .

Solution is presented graphically [25] for Fourier number $F_0 = \frac{k^*t}{a^2}$. It shows that times of propagation of heat in sand and water are of same order, but heat propagates through the steam faster by two orders. Comparison with time of water penetration into the layer gives the following:

- time of water penetration through 20 cm layer (from top or bottom) is 800 sec (maximum velocity, Table 3);
- time of heat propagation through sand or water is 100 sec;
- time of heat propagation through steam is 1 sec.

In other words it shows that when water penetrates about 2.5 mm inside the bed, the heat front can propagate on 0.2 m through the steam, from the middle of layer to it's boundaries. Such a ratio of propagation times can be taken as criteria for choosing of heat removal mechanism. It is clear that this ratio is depending on characteristics of the system such as geometry, thermophysical properties and initial water penetration condition (flow rate).

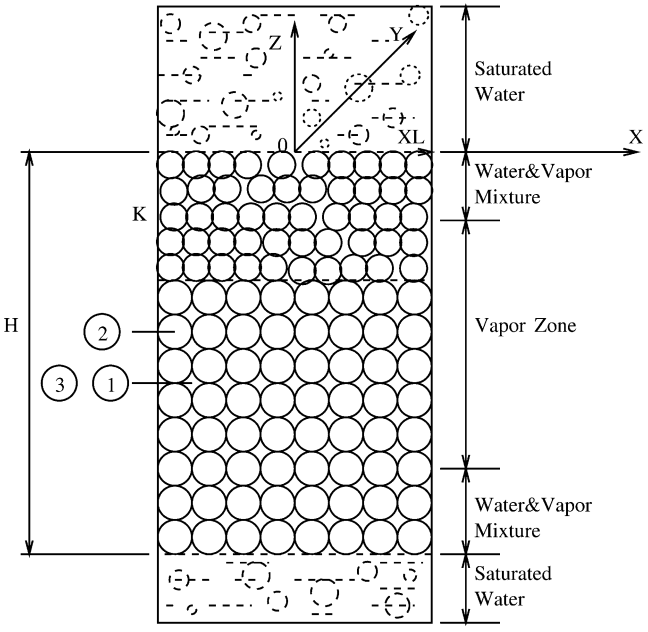

Fig. 2. Steam flow configuration.

Table 3
Results of calculations of flow rates in different particle beds

Bed parameters	$U_{w,layer}$, m·s^{-1}	$L_{vaporiz}$, m (at 20 KW)	G_{calc} kg·s^{-1}	G_{exp} kg·s^{-1}
$\varepsilon = 0.4$ $D_{mean} = 0.2$ mm	1×10^{-4}	3×10^{-8}	0.01	0.01
$\varepsilon = 0.36$ $D_{mean} = 0.9$ mm	2.4×10^{-4}	9×10^{-7}	0.02	0.019
$\varepsilon = 0.26$ $D_{mean} = 0.8$ mm	2×10^{-4}	3×10^{-7}	0.012	0.0115

Table 4
Thermophysical properties of materials used in calculations

Material	Thermal conductivity, W·m^{-1}·K^{-1}	Density, kg·m^{-3}	Heat capacity, J·kg^{-1}·K^{-1}
sand	0.27	1515	800
water	0.68	1000	4200
steam	0.025	0.58	2060

Finally, in establishing a model for analyzing this problem, the following assumptions were employed:

- the fluid phase is single phase and is compressible (steam);
- the particle sizes are significantly larger than molecular-kinetic sizes, but they are significantly less than characteristic size of the system;
- the physical properties such as thermal conductivity coefficient, dynamic viscosity etc. are temperature dependent;
- solid particles are immovable and porosity is constant in each layer.

3.2. Mathematical formulation of the problem

Employing the equations of the saturated granular layer which were introduced by Nigmatulin [26] and then developed by Kazachkov [27] for two-dimensional case; the mathematical model of this system can be presented as follows:

Mass balance equation:

$$\frac{\partial \rho_1^0}{\partial t} = -\rho_1^0\left(\frac{\partial u_1}{\partial x} + \frac{\partial w_1}{\partial z}\right) \tag{1}$$

Momentum equations:

$$\rho_1 \frac{\partial \vec{v}}{\partial t} + \nabla p_1 + (\rho_1 + \rho_2)\vec{g} = \nabla \sigma_k \tag{2}$$

$$\rho_1^0(1 + 0.5\alpha_2)\frac{\partial \vec{v}}{\partial t} + \nabla p_1 + \mu_1 \frac{\vec{v}}{K_0}\left(\frac{\alpha_1}{\alpha_{10}}\right)^{-n} + \rho_1^0 \vec{g} = 0 \tag{3}$$

Energy equations:

$$\rho_1 C_{v1}\left(\frac{\partial T_1}{\partial t} + \vec{v}\nabla T_1\right) = \alpha_1 R T_1 \frac{\partial \rho_1^0}{\partial t} + \nabla(k_1 \nabla T_1) + Q_\Sigma + Q_V + \mu_1\left(u_1^2 + w_1^2\right)\frac{\alpha_1}{K} \tag{4}$$

$$\rho_j C_j \frac{\partial T_j}{\partial t} = \nabla(k_j \nabla T_j) + (j-3)Q_\Sigma \tag{5}$$

where $j = 2, 3$, $K = K_0(\alpha_1/\alpha_{10})^n$, $k_1 = \mu_1 \frac{C_{p1}}{Pr}$, $\frac{\mu_1}{\mu_{10}} = (\frac{T_1}{T_{10}})^m$ with Prandtl number taken at μ_{10} and $m = 0.5$–1.0.

The values with "0" indexes are taken at the fixed temperature T_{j0}. At such conditions the velocity component is calculated as follows:

$$w_1 = \left(\rho_1 + \rho_2 - \rho_1^0\right)\frac{gK}{\mu_1}$$

The above expression for the vertical velocity component w_1 corresponds, in the first order approximation, to the Darcy's law when $\rho_1^0 \ll \rho_1 + \rho_2$. The Darcy's law can also be employed, when u_1 the horizontal component is much smaller in comparison with w_1 the vertical component of the velocity.

3.3. Boundary conditions

The initial conditions of this system are taken as following:

$$t = 0, \qquad p_1 = p_1^0, \qquad \alpha_1 = \alpha_1^0, \qquad T_j = T_j^0$$

Later, the initial conditions may suffer perturbations, which may make them decrease or increase.

The system is symmetrical relative to the vertical axis and at the right boundary the horizontal velocity is zero:

$$x = x_L, \qquad u_1 = 0$$

The condition of temperature and heat flux equilibrium at the boundary with unpermeable surrounding and with $\alpha_1 \sim \alpha_2$ and $k_1 \ll k_2$ gives:

$$x = x_L, \qquad k_2 \frac{\partial T_2}{\partial x} = k_3 \frac{\partial T_3}{\partial x}$$

When we have $x = x_\infty$

$$\frac{\partial T_3}{\partial x} = 0$$

At the lower boundary $z = -H$ the temperatures are:

$$T_j = T_{jH}$$

A boiling water pool occurs at the upper layer of the system and at the bottom, hence:

$$z = 0, \qquad T_j = T_{jH}$$

3.4. Non-dimensional formulation of the problem

The following length, time, velocity, pressure and temperature scales were introduced: H, H^2/a_2^0, a_2^0/H^2, $\mu_{10}a_2^0/K_c$ and ΔT, where ΔT is the characteristic change of temperature in the system. Eqs. (1)–(5) for the case $\alpha_1 = \text{const}$ can be rewritten as:

$$u_1 = -\left(\frac{T_{10}}{T_1}\right)^m \frac{\partial p_1}{\partial x}, \qquad \frac{\partial \rho_1^0}{\partial Fo} = -\rho_1^0\left(\frac{\partial u_1}{\partial x} + \frac{\partial w_1}{\partial z}\right) \tag{6}$$

$$w_1 = \left(\rho_1 + \rho_2 - \rho_1^0\right)\frac{gK}{\mu_1} \tag{7}$$

$$\frac{\partial p_1}{\partial z} = Pe(\alpha_1 - 1)\left(1 - \Delta_2(T_2 - T_{20})\right) - Re_*^2 \frac{\alpha_1 p_1}{T_1} \tag{8}$$

$$\begin{aligned}\frac{\partial T_1}{\partial Fo} = {} & (1-\gamma_1)T_1\left(\frac{\partial u_1}{\partial x} + \frac{\partial w_1}{\partial z}\right) - \left(u_1\frac{\partial T_1}{\partial x} + w_1\frac{\partial T_1}{\partial z}\right) \\ & + (\gamma_1 - 1)\left(u_1^2 + w_1^2\right)\left(\frac{T_1}{T_{10}}\right)^m \frac{T_1}{p_1} \\ & + \frac{\gamma_1 Pe(T_1/T_{10})^m}{\alpha_1 \kappa_a \kappa_p Re_*^2 p_1}\left[T_1\left(\frac{\partial^2 T_1}{\partial x^2} + \frac{\partial^2 T_1}{\partial z^2}\right)\right. \\ & \left. + m\left[\left(\frac{\partial T_1}{\partial x}\right)^2 + \left(\frac{\partial T_1}{\partial z}\right)^2\right] + \xi Nu_1 T_1(T_2 - T_1)\right],\end{aligned} \tag{9}$$

$$\frac{\partial T_2}{\partial Fo} = \frac{1/(1-\alpha_1)}{1-\Delta_2(T_2-T_{20})} \times \left[\frac{\partial^2 T_2}{\partial x^2} + \frac{\partial^2 T_2}{\partial z^2} + Nu_1 \frac{\xi}{\kappa_k}\left(\frac{T_1}{T_{10}}\right)^m (T_1 - T_2)\right] \tag{10}$$

$$\frac{\partial T_3}{\partial Fo} = a_{32}\left(\frac{\partial^2 T_3}{\partial x^2} + \frac{\partial^2 T_3}{\partial z^2}\right) \tag{11}$$

$$Fo = 0, \qquad p_1 = p_1^0, \qquad T_j = T_j^0 \tag{12}$$

$$x = x_\infty, \qquad \frac{\partial T_3}{\partial x} = 0 \tag{13}$$

$$x = x_L, \qquad u_1 = 0, \qquad \frac{\partial T_2}{\partial x} = a_{32}\frac{\partial T_3}{\partial x} \tag{14}$$

$$z = 0, \qquad T_j = T_{jH} \tag{15}$$

$$z = -1, \qquad T_j = T_{jH} \tag{16}$$

where $Pe = w_0 H/a_2^0$—Peclet number; $w_0 = \rho_{20}^0 Kg/\mu_{10}$; $\rho_1^0 = \kappa_\rho \frac{Re_*^2 p_1}{Pe T_1}$; $w_1 = (1-\alpha_1)[Pe - \kappa_\rho Ra^*(T_2 - T_{20}) - Re_*^2 \frac{p_1}{T_1}](\frac{T_{10}}{T_1})^m$; $Re_v = w_0 b_1/\nu_{10}$—Reynolds number in voids; $Re_*^2 = \frac{gH}{R\Delta T}$; $Da = K/H^2$—Darcy number; $Gr = g\Delta_2 H^3/\nu_{10}^2$—Grasshoff number; $Ra^* = Gr\,Pr^* Da$—Rayleigh number; $Nu_1 = 2 + 0.6 Pr^{1/3} Re_v^{1/2}$—Nusselt number; $\kappa_a = a_2^0/a_1^0$; $\kappa_\rho = \rho_{20}^0/\rho_{10}^0$; $a_1^0 = k_1^0/C_1\rho_{10}^0$; $Fo = a_2^0 t/H^2$—Fourier number; $\Delta_2 = \Delta T \beta_{T2}$; $\gamma_1 = C_{p1}/C_{v1}$; $\kappa_k = k_2/k_1^0$; $a_{32} = a_3/a_2^0$; $\xi = s_{12}H^2/b_1$—parameters of the structure of the granular layer; s_{12}—specific interface area, $b_1 = b\sqrt{2(2-\pi/3)\pi}$—void radius, b—particle radius.

In this system three different conditions are present: non-thermal equilibrium between fluid and solid, system non-linearity and non-linearity of the physical properties. The first condition is shown by the term $\xi(T_1 - T_2)$. However, it should be noted that there is some limitation to the ξ parameter. The energy equations have the term $\xi(T_1 - T_2)$, which at the small particle sizes, big linear system sizes and, if fluid and solid temperatures are close enough, will hold an uncertainty of the "$\infty \cdot 0$" type. The term $m[(\frac{\partial T_1}{\partial x})^2 + (\frac{\partial T_1}{\partial z})^2]$ might cause the escalation of heat processes in local space because of non-linearity of the thermal conductivity coefficient. This phenomenon was investigated by Samarsky [28] as an example of solution of the one-dimensional heat conduction problems with non-linear thermal conductivity coefficient.

3.5. Solution procedure

The problem (6)–(15) were solved employing the finite-difference scheme based on the split step method described by Janenko [29]. Spliting between spatial variables transformed the two-dimensional problem to two onedimensional problems:

On the lower limit of the time step:

$$\frac{\partial \rho_1^0}{\partial Fo} = -2\rho_1^0 \frac{\partial u_1}{\partial x} \tag{17}$$

$$\frac{1}{2}\frac{\partial T_1}{\partial Fo} = (1-\gamma_1)T_1\frac{\partial u_1}{\partial x} - u_1\frac{\partial T_1}{\partial x} + (\gamma_1 - 1)u_1^2\left(\frac{T_1}{T_{10}}\right)^m \frac{T_1}{p_1} + \frac{\gamma_1 Pe(T_1/T_{10})^m}{\alpha_1\kappa_a\kappa_p Re_*^2 p_1}\left[T_1\frac{\partial^2 T_1}{\partial x^2} + m\left(\frac{\partial T_1}{\partial x}\right)^2 + \alpha\xi Nu_1 T_1(T_2 - T_1)\right] \tag{18}$$

$$\frac{1}{2}\frac{\partial T_2}{\partial Fo} = \frac{1/(1-\alpha_1)}{1-\Delta_2(T_2-T_{20})} \times \left[\frac{\partial^2 T_2}{\partial x^2} + Nu_1\alpha\frac{\xi}{\kappa_k}\left(\frac{T_1}{T_{10}}\right)^m (T_1 - T_2)\right] \tag{19}$$

$$\frac{\partial T_3}{\partial Fo} = 2a_{32}\frac{\partial^2 T_3}{\partial x^2} \tag{20}$$

On the upper limit of the time step:

$$\frac{\partial \rho_1^0}{\partial Fo} = -2\rho_1^0 \frac{\partial w_1}{\partial z} \tag{21}$$

$$\frac{1}{2}\frac{\partial T_1}{\partial Fo} = (1-\gamma_1)T_1\frac{\partial w_1}{\partial z} - w_1\frac{\partial T_1}{\partial z} + (\gamma_1 - 1)w_1^2\left(\frac{T_1}{T_{10}}\right)^m \frac{T_1}{p_1} + \frac{\gamma_1 Pe(T_1/T_{10})^m}{\alpha_1\kappa_a\kappa_p Re_*^2 p_1} \times \left[T_1\frac{\partial^2 T_1}{\partial z^2} + m\left(\frac{\partial T_1}{\partial z}\right)^2 + (1-\alpha) \times \xi Nu_1 T_1(T_2 - T_1)\right] \tag{22}$$

$$\frac{1}{2}\frac{\partial T_2}{\partial Fo} = \frac{1/(1-\alpha_1)}{1-\Delta_2(T_2-T_{20})} \times \left[\frac{\partial^2 T_2}{\partial z^2} + Nu_1(1-\alpha)\frac{\xi}{\kappa_k}\left(\frac{T_1}{T_{10}}\right)^m (T_1 - T_2)\right] \tag{23}$$

$$\frac{\partial T_3}{\partial Fo} = 2a_{32}\frac{\partial^2 T_3}{\partial z^2} \tag{24}$$

where $\alpha = [0; 1]$ is an approximation parameter.

Differentials inside the two-dimensional area are approximated with the central differences of the second order:

$$\frac{\partial f}{\partial x} \sim \frac{f_n^{i+1,j} - f_n^{i-1,j}}{2h_x}$$

$$\frac{\partial^2 f}{\partial x^2} \sim \frac{f_n^{i+1,j} - 2f_n^{i,j} + f_n^{i-1,j}}{h_x}$$

and on the boundary:

$$\frac{\partial f}{\partial x} \sim \frac{f_n^{3,j} - 2f_n^{2,j} + f_n^{1,j}}{2h_x}$$

Relative to "z" coordinate the same operations have to be made. To calculate differential in time the following expression is employed:

$$\frac{\partial f}{\partial F_0} \sim \frac{f_{n+1} - f_n}{\tau}$$

4. Examples of calculated results

In all of the POMECO tests a stable local dryout was observed, which confirmed the assumption about an escalation of temperature in space. We assumed that at high enough heat generation the governing cooling mechanism becomes steam cooling. The homogeneous and stratified POMECO tests with one downcomer were analyzed using the model presented above. The initial temperature perturbations were set as a *sine*function:

$$T_1^0(x,z) = T_{10}^0(x,z) + \Theta_1^0 \sin k_1 x \sin m_1 z$$

where $T_{10}^0(x,z)$ is the uniform temperature distribution, Θ_1^0—the perturbation amplitude, k_1, m_1—wave numbers. Calculations were performed using the 21×51 grid.

The first examination was performed for the homogeneous test (homo-1.2) with mean particle size of 0.2 mm and porosity of 0.4. Fig. 3 depicts the space distribution of the dimensionless temperature difference. As it can be seen, except the temperature peak, some increase in temperature near the wall was obtained. It can be explained by the zero heat flux boundary condition, which was set at the side wall. Fig. 4 presents the comparison between the model prediction and experimental results, they are in reasonable agreement.

Three stratified tests (strat-1.2, strat-2.2, strat-3.2) were analyzed, in which different particle layers for simulation of debris bed were employed. It should be noted that, basically, these tests are quite similar in term of porosity numbers and power density. However, there are some differences compared to the homogeneous case.

As it can be seen from the Table 5 the dryout locations in the tests homo-1.2 and strat-3.2 are very close, what was confirmed by calculations (Figs. 9 and 10). The bed in the test strat-3.2 consists of two layers: lower layer (130 mm height) formed from the sand particles with mean diameter of 1 mm and porosity of 0.36, and upper layer (240 mm height), which is the same as in the test homo-1.2.

Positions of dryout in the test strat-1.2 and strat-2.2 are higher than in the tests described above. In these experiments the bigger lower layers with height of 240 mm were produced from the sand particles with mean diameter of 1 mm and porosity of 0.36, which is lower than porosity of thicker layers in the tests homo-1.2 and strat-3.2. The decrease in porosity could lead to increase of the pressure drop inside the bed, because the water supply from the bottom was the same in all experiments. The increase of the pressure drop can enhance the steam velocity and intensify cooling process, which led to movement of dryout position to the top. But due to the different compositions of upper layers in these tests the power densities, at which the beginnings of dryout were observed, were different. In the test strat-1.2 the upper layer (130 mm) was built using the sand particles with mean size of 0.2 mm and porosity of 0.4 and in this case the dryout power density was 0.5 MW·m^{-3}. In the case of strat-2.2 the upper layer had mean particle size 0.8 mm and porosity 0.26 and this layer provided enhanced thermal resistance compared to strat-1.2, what led to decrease in the dryout power density to 0.4 MW·m^{-3}. The results of these calculations are presented in Figs. 5, 6, 7 and 8.

Table 5
Dryout locations in POMECO tests with one downcomer

Test	Dryout heat flux KW·m^{-2}	Temperature in the dry zone, °C	Dryout location X, Z coordinate, mm
homo-1.2	186	151	$X = 30$, $Z = 140$
strat-1.2	187	123	$X = 30$, $Z = 180$
strat-2.2	138	160	$X = 90$, $Z = 180$
strat-3.2	190	155	$X = 30$, $Z = 100$

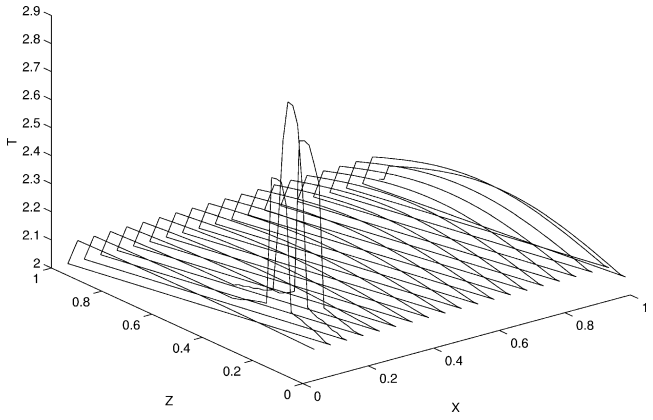

Fig. 3. Temperature distribution in the bed (test homo-1.2). Calculations performed at the power density 0.5 MW·m^{-3}.

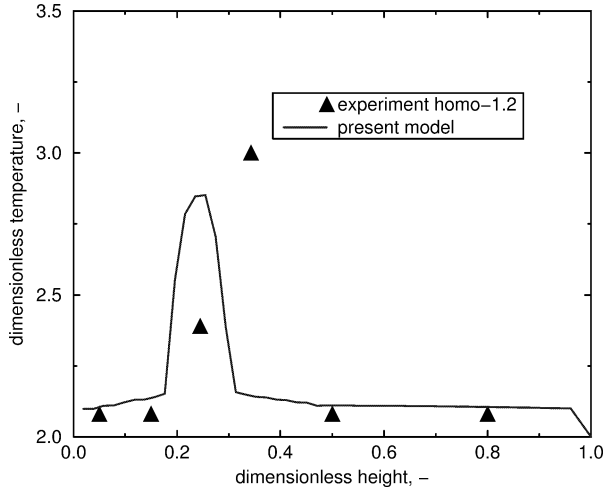

Fig. 4. Temperature distribution along Z-axis at $X = 0.2$.

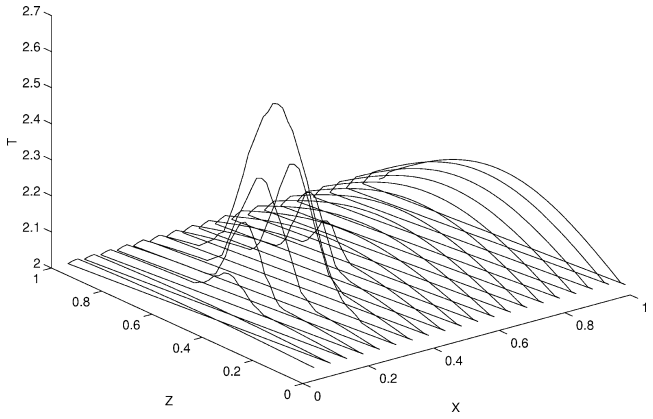

Fig. 5. Temperature distribution in the bed (test strat-1.2). Calculations performed at the power density 0.5 MW·m^{-3}.

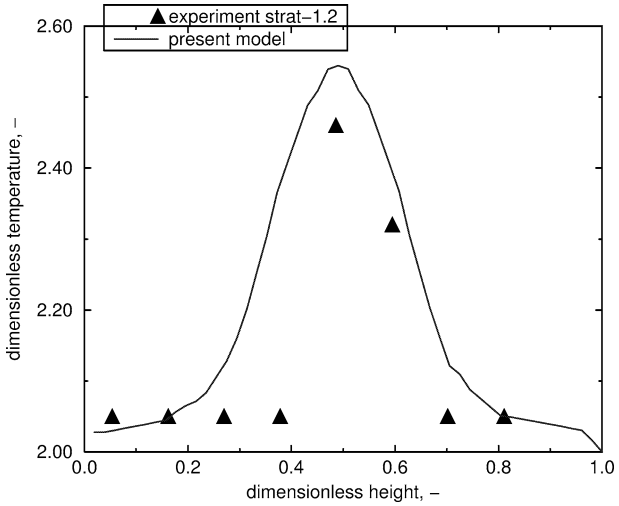

Fig. 6. Temperature distribution along Z-axis at $X = 0.2$.

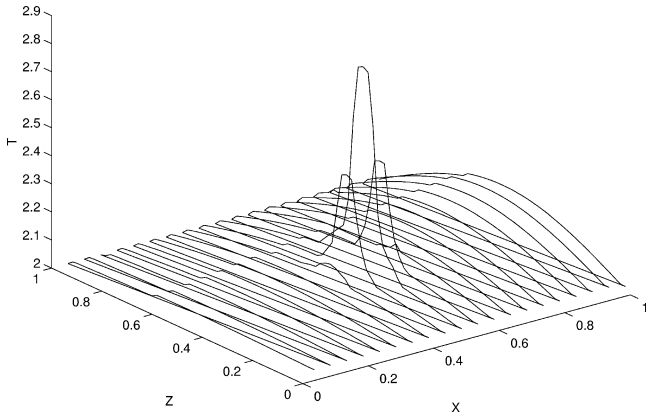

Fig. 7. Temperature distribution in the bed (test strat-2.2) Calculations performed at the power density 0.4 MW·m^{-3}.

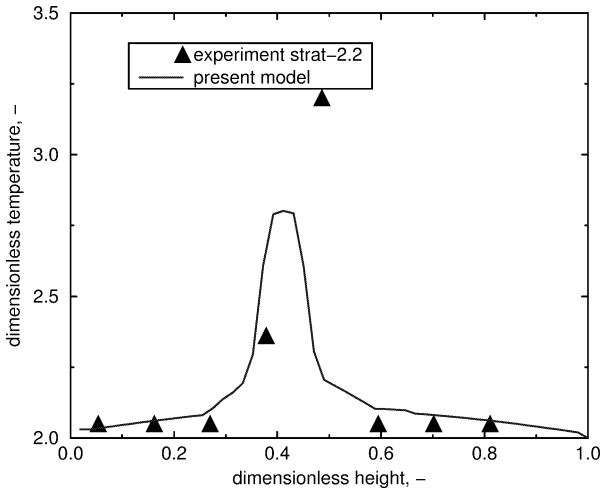

Fig. 8. Temperature distribution along Z-axis at $X = 0.2$.

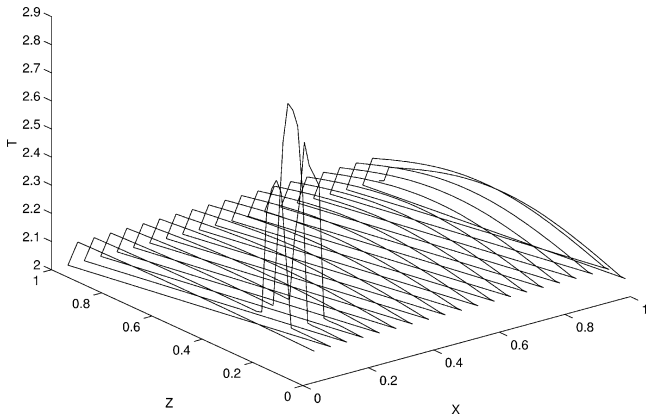

Fig. 9. Temperature distribution in the bed (test strat-3.2) Calculations performed at the power density 0.5 MW·m^{-3}.

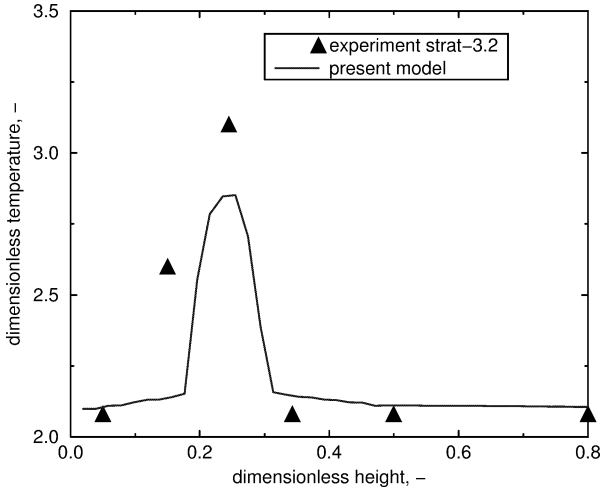

Fig. 10. Temperature distribution along Z-axis at $X = 0.2$.

Table 6
Properties used in calculations

Property	Steam	Sand particles
Density, kg·m^{-3}	0.58	1515
Conductivity, W·(mK)$^{-1}$	25.0×10^{-3}	0.27
Heat diffusivity, m^2·s^{-1}	2.04×10^{-5}	2.2×10^{-7}
Dynamic viscosity, Pa·s	1.24×10^{-7}	–
Temperature drop in the system ΔT, °K	50	
Total layer height, m	0.35	

Comparison between the experimental and calculated results of the tests homo-1.2 and strat-3.2, strat-1.2 and strat-2.2 show that the thermal behavior of stratified beds is determined by the composition of the dominating layer.

Properties used in calculations are presented in the Table 6.

5. Summary

An innovative aspect of the particulate debris bed dry out experiments in the POMECO facility was the introduction of downcomer in the bed which enabled the water overlayer to supply water to the bottom of the debris bed where it would flow co-current with the steam produced. It was found the provision of downcomers enhanced the magnitude of dry out heat flux several times.

A model of steam flowing through a saturated porous medium with internal heat generation was described. Some of POMECO experiments performed at RIT were analyzed with this model. The calculated results agree with the measurements on dryout location with reasonable accuracy. The dryout is understood to be caused by escalation of heat transfer in local area because of non-linear dependence of thermal conductivity coefficient (with power factor of 0.5) in critical regimes. In reality, the physical situation is much more complicated: two-phase flow in porous media with local phase change, variable boundary conditions depending on flow regimes, etc. Nevertheless, in the heat escalation cases it may be assumed the local steam temperature grows so fast that the dryout position is predetermined by the thermodynamic processes in the steam flow.

References

[1] D. Magalon et al., The FARO programme recent results and synthesis, CSARP Meeting, USA, Bethesda, Maryland, May, 1997.

[2] M.V. Choudhary, N.M. El-Wakil, Heat transfer and flow characteristics in conductive porous media with energy generation, in: Proc. Internat. Heat Transfer Conf., Versailles, France, 1970.

[3] V. Dhir, I. Catton, Dryout heat fluxes for inductively heated particulate beds, J. Heat Transfer 99 (May) (1977).

[4] L.L. Vasiliev, V.A. Mairov, An analytical study of resistance, heat transfer and stability in evaporative cooling of a porous heat producting element, Internat. J. Heat Mass Transfer 12 (1979) 301–307.

[5] V.M. Polyaev, V.A. Mairov, L.L. Vasiliev, Hydrodynamic and Heat Transfer in the Porous Elements of the Avionic Components, Moscow, Mashinostroenie, 1988.

[6] A.S. Naik, V.K. Dhir, Forced flow evaporative cooling of a volumetrically heated porous layer, Internat. J. Heat Mass Transfer 25 (4) (1982) 541–552.

[7] G. Hofmann, On the location and mechanisms of dryout in top-fed and bottom-fed particulate beds, Nuclear Technology 65 (1984).

[8] T. Schulenberg, U. Muller, A refined model for the coolability of core debris with flow entry from the bottom, Presented at the 6th Information Exchange Mig on Debris Coolability, Univ. of California, Los Angeles, 1984.

[9] F.P. Tsai, Dryout heat flux in a volumetrically heated porous bed, Ph.D. Dissertation, Univ. of California, Los Angeles, 1987.

[10] V.X. Tung, V.K. Dhir, A hydrodynamic model for two-phase flow through porous media, Internat. J. Multiphase Flow 14 (1) (1988) 47–65.

[11] V.X. Tung, V.K. Dhir, Finite element solution of multi-dimensional two-phase flow through porous media with arbitrary heating conditions, Internat. J. Multiphase Flow 16 (6) (1990) 985–1002.

[12] R.J. Lipinski, A model for boiling and dryout in particle beds, Sandia Labs, SAND 82-9765, NUREG/CR-2646, 1982.

[13] R.J. Lipinski, A coolability modal for post accident nuclear reactor debris, Nuclear Technology 65 (1984) 53–66.

[14] A.K. Stubos, J.-M. Buchlin, Modeling of vapor channeling behavior in liquid-saturated debris bed, Trans. ASME 110 (1988)(November).

[15] A.K. Stubos, J.-M. Buchlin, Vapor channels in boiling, unconstricted particle beds-effect on the dryout heat flux, Internat. J. Multiphase Flow 20 (1) (1994) 131–152.

[16] A.K. Stubos, J.-M. Buchlin, Analysis and numerical simulation of the thermohydraulic behavior of a heat dissipating debris bed during power transients, Internat. J. Heat Mass Transfer. 36 (5) (1993) 1391–1401.

[17] M. Sözen, K. Vafai, Analysis of the non-thermal equilibrium condensing flow of a gas through a packed bed, Internat. J. Heat Mass Transfer 33 (6) (1990) 1247–1261.

[18] A.V. Kuznetsov, An investigation of a wave of temperature difference between solid and fluid phases in a porous packed bed, Internat. J. Heat Mass Transfer 37 (18) (1994) 3030–3033.

[19] A.V. Kuznetsov, Investigation of multi-dimensional effects during heating a porous packed bed, in: 2nd European Thermal-Sciences and 14th UIT National Heat Transfer Conference, 1996.

[20] A.V. Kuznetsov, Thermal nonequilibrium forced convection in porous media, in: D.B. Ingham, I. Pop (Eds.), em Transport Phenomena in Porous Media, Elsevier, Oxford, 1998, pp. 103–129.

[21] M.J. Konovalikhin, Z.L. Yang, M. Amjad, B.R. Sehgal, On dryout heat flux of s particle debris bed with a downcomer, in: ICONE-8, Baltimore, USA, April, 2000.

[22] H. Alsmeyer, B. Spencer, W. Tromm, The COMET concept for cooling of ex-vessel corium melts, in: ICONE-6, USA, San Diego, 1998.

[23] M. Becker, J. Engström, R.V. Macbeth, Enhancement of core debris coolability, TIT-Report: KTH-NEL-51, 1990.

[24] F.P. Incropera, D.P. DeWitt, Fundamentals of Heat and Mass Transfer, 4th Edition, New York, 1995.

[25] H.S. Carslaw, J.C. Jaeger, Conduction of Heat in Solids, 2nd Edition, Oxford University Press, London, 1962.

[26] R.I. Nigmatulin, The Base of Mechanics of Heterogeneous Media, Nauka, Moscow, 1978.

[27] I.V. Kazachkov, On the mathematical simulation of processes of nonstationary nonisothermal filtration in geothermal systems, J. Numer. Appl. Math. 60 (1986).

[28] A.A. Samarsky et al., Regimes With Peaks in the Problem for Quasilinear Parabolic Equations, Nauka, Moscow, 1987.

[29] N.N. Janenko, The Split Step Method for Solution of the Multidimensional Problems of Mathematical Physics, Nauka, Novosibirsk, 1967.